Sensors & Actuators: B. Chemical 417 (2024) 136056

Contents lists available at ScienceDirect

Sensors and Actuators: B. Chemical

journal homepage: www.elsevier.com/locate/snb

Dual-drive strategy-based modulation of the interfacial charge of S-scheme heterojunction and photoelectrochemical ultrasensitive detection of CD44

Yamei Li [a], Xuan Kuang [a], Faying Li [b], Hongmin Ma [a], Dan Wu [a], Hongying Jia [a,*], Tingting Wu [a,*], Huangxian Ju [a,c], Qin Wei [a,d,**]

[a] Collaborative Innovation Center for Green Chemical Manufacturing and Accurate Detection, Key Laboratory of Interfacial Reaction & Sensing Analysis in Universities of Shandong, School of Chemistry and Chemical Engineering, University of Jinan, Jinan 250022, PR China
[b] School of Chemistry and Pharmaceutical Engineering, Shandong First Medical University & Shandong Academy of Medical Sciences, Taian 271016, PR China
[c] State Key Laboratory of Analytical Chemistry for Life Science, School of Chemistry and Chemical Engineering, Nanjing University, Nanjing 210023, PR China
[d] Department of Chemistry, Sungkyunkwan University, Suwon 16419, Republic of Korea

ARTICLE INFO

Keywords:
Dual-drive strategy
Thermal energy
Sulfur vacancies
S-scheme heterojunction
PEC biosensor

ABSTRACT

The efficacy of charge carrier separation plays a crucial role in influencing the practical application of photoelectrochemical (PEC) detection platforms, which can be meticulously engineered to realize highly sensitive detection at the sensing interface. Hence, a novel dual-drive strategy was proposed to integrate thermally-assisted external drive behavior with the internal drive behavior of sulfur vacancies (SVs), realizing the rapid separation of charge at the S-scheme heterojunction sensing interface. On the one hand, unabsorbed solar energy was utilized an external driving force to facilitate efficient photothermoelectric conversion within the In_2S_3/CdS heterojunction, achieving the photocurrent response intensity 1.5 times higher than conventional PEC detection methods. On the other hand, introducing sulfur vacancies (SVs) as internal driving forces induced ordered migration and directional flow of charge carriers. Moreover, density functional theory (DFT) calculations and experimental results demonstrated that photo-generated carriers achieved rapid separation along the S-scheme heterojunction. Under the optimal conditions, a biosensor constructed based on the dual-drive strategy exhibited high sensitivity for the CD44 (cluster of differentiation-44) cluster, with a low detection limit of 0.132 pg $mL^{-1}$and a wide linear range of 0.001 ~ 1000 ng mL^{-1}. The proposed strategy offers new insights into how to effectively harness excess energy in the traditional ultraviolet spectral range for ultrasensitive biosensors.

1. Introduction

Cluster of differentiation-44 (CD44), as a cell surface transmembrane glycoprotein, is over-expressed in many cancers through cell adhesion, migration, proliferation, differentiation and signal transduction, which seriously endangers human health [1,2]. Clinical medicine have indicated that the effective detection of CD44 antigen may become the key to explore the diagnosis of breast cancer [2]. As an emerging detection method, photoelectrochemical (PEC) biosensing analysis realizes the quantification of targets through the PEC responses generated by the combination of semiconductor materials and specific biometric recognition elements. Compared with methods such as enzyme-linked adsorption and surface-enhanced Raman scattering, the PEC technique enables highly efficient detection and provides a new perspective for clinical diagnosis [3]. The separation efficiency and migration rate of photo-generated carriers in semiconductor materials are crucial factors that impact the PEC response of sensing platforms [4]. To construct a high-sensitivity PEC sensor, researchers employ various methods such as constructing heterojunctions, introducing defects, and utilizing catalysts to enhance the photoelectric conversion performance of the detection platform [5–7]. For example, Jia et al. developed a molecularly imprinted PEC biosensor utilizing the In_2O_3/Bi_2S_3 S-scheme heterojunctions, demonstrating excellent detection capability for florfenicol (FF) [8]. Yin et al. introduced vacancy engineering in the $CdIn_2S_4$/CdS S-scheme heterojunction to realize selective photocatalytic oxidation of toluene [9]. Despite the significant progress of these sensing strategies in

* Corresponding authors.
** Corresponding author at: Collaborative Innovation Center for Green Chemical Manufacturing and Accurate Detection, Key Laboratory of Interfacial Reaction & Sensing Analysis in Universities of Shandong, School of Chemistry and Chemical Engineering, University of Jinan, Jinan 250022, PR China.
E-mail addresses: Hongying187@163.com (H. Jia), wuting7692@163.com (T. Wu), sdjndxwq@163.com (Q. Wei).

https://doi.org/10.1016/j.snb.2024.136056
Received 30 April 2024; Received in revised form 26 May 2024; Accepted 30 May 2024
Available online 3 June 2024

improving the PEC performance, the limitation of the spectral utilization range of photoactive materials still constrains the further improvement of the photoelectric conversion efficiency in PEC sensing platforms.

Most photoactive materials primarily focus on the utilization of energy in the UV–visible region, therefore enhancing the exploitation of energy in other spectral ranges holds promise for improving photoelectric conversion efficiency [10,11]. Recent studies have found that integrating nanomaterials with photothermal and thermoelectric conversion properties in the same analytical platform can effectively exploit excess thermal energy to enhance photocatalytic performance [12,13]. Inorganic nanomaterials (e.g., two-dimensiona nanomaterials, transition metal sulfides, etc.) exhibit higher photoelectric conversion efficiencies due to better water solubility as well as photostability [14]. For instance, Liu et al. used reduced graphene oxide (rGO) to improve the catalytic rate significantly by thermally assisted photocatalytic reduction of CO_2 [15]. Li et al. applied the pyroelectric material of CdS into the field of photocatalytic hydrogen evolution, which reduced the use of noble metals and improved the apparent quantum efficiency, demonstrating the feasibility of the pyroelectric effect to enhance photocatalytic efficiency [16]. Therefore, rationally utilizing the potential of solar energy and transcending the limitation of solar energy spectra, the thermally assisted photocatalytic behavior provides a viable pathway for the early realization of practical applications of PEC sensing platforms [17].

Inspired by the above results, a dual-drive sensing platform for the ultrasensitive detection of CD44 was developed based on S-scheme heterojunction constructed from In_2S_3/CdS (Scheme 1). The photothermal agent In_2S_3 synergized with the pyroelectric material CdS to efficiently convert unutilized light energy into thermal energy, providing a strong external driving force for the efficient separation of electrons and holes [18]. Meanwhile, the effective regulation of interfacial charge was realized by using sulfur vacancies (SVs) as the internal driving force of the system. In summary, the externally driven mechanism of thermal energy synergized with the internally driven mechanism of SVs through the ordered pathways provided by the S-scheme heterojunction jointly contributed to the direction of carrier migration and the separation rate at the heterojunction interface [19]. The dual-drive strategy fully utilized the excess energy of solar energy to construct the PEC sensor with high detection performance, which provides a new idea for sensing technology.

2. Experimental section

2.1. Materials and instruments

The antigens and antibodies used in this experiment, such as CD44 and anti-CD44, are all from Wuhan Fine Biotech Co., Ltd. Additional information can be found in the supporting information.

2.2. Synthesis of In_2S_3 and CdS

In_2S_3 was synthesized by a typical one-pot hydrothermal method [20]. The preparation process of In_2S_3 is shown in Scheme 1A. 0.8 mmol of $InCl_3$ with 1.6 mmol of TAA was dissolved in 30 mL of a mixed solution of ethanol and deionized water with a volume ratio of 1:1. After stirring for 30 min, the solution was heated at 180 °C for 24 h. The samples were collected after natural cooling, washed and dried.

CdS was prepared by hydrothermal synthesis [21]. 0.01 mmol of Cd $(NO_3)_2{\cdot}4\ H_2O$ was added to 40 mL of ethanol and stirred with the same molar ratio of thiourea. The mixture was heated at 150 °C for 24 h. The sample was washed several times by centrifugation and dried under vacuum.

2.3. Photoelectrical sensing of CD44

The process of constructing the dual-drive PEC sensing platform is described in Scheme 1A. To introduce CdS hollow spheres after modifying In_2S_3 nanoflowers on bare indium tin oxide (ITO) electrodes. Carboxyl-containing thioglycolic acid (TGA) provided the carboxyl group, and 1-(3-dimethylaminopropyl)-3-ethyl carbodiimide hydrochloride (EDC)/N-hydroxysuccinimide (NHS) was used for the activation of the carboxyl group to achieve antibody connection. After incubation with a certain concentration of capture antibody (Ab), bovine serum albumin (BSA) was introduced to block the non-specific site to avoid unnecessary interference. Then, the PEC sensor was successfully constructed by adding different concentrations of CD44. A phosphate buffer solution (PBS) containing 0.1 mol L^{-1} ascorbic acid (AA) was added to the aluminum foil-wrapped electrolytic cell and PEC

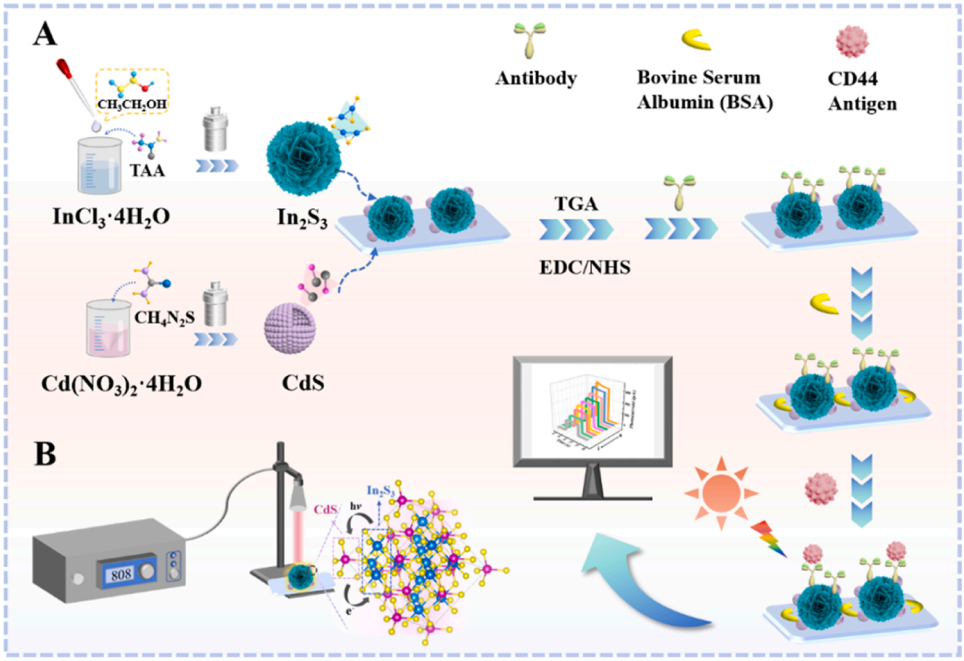

Scheme 1. (A) Synthesis of In_2S_3, CdS and fabrication steps of the PEC sensing platform. (B) Photothermal detection schematic diagram.

was measured using a three-electrode system. In addition, the sensor was irradiated by an 808 nm near-infrared laser (1.5 w cm^{-2}) for 140 s to verify the photothermoelectric effect on its performance (Scheme 1B).

3. Results and discussion

3.1. Characterization of In_2S_3, CdS and In_2S_3/CdS

Scanning electron microscopes (SEM) and transmission electron microscopes (TEM) were used to characterize the structure and morphology of materials. Initially, In_2S_3 displayed nanoflowers with diameters of about 3 ~ 5 μm, containing ruffled petals that facilitated uniform material dispersion (Fig. 1A). In Fig. 1B, the CdS exhibited a hollow sphere morphology with a diameter of approximately 300 nm, which reduced the diffusion path length of photo-generated carriers and improved the charge transfer efficiency. The uniformly loaded CdS hollow spheres on the surface of In_2S_3 nanoflowers could be observed in Fig. 1C. The change of crystalline phase after composite was analyzed by X-Ray Diffraction (XRD) diffraction pattern (Fig. 1D). No shifts of the In_2S_3/CdS composite diffraction peaks shifted, but the crystallinity decreased, indicating the composite had high concentration defects [22]. Furthermore, Fig. 1E observed CdS hollow spheres loaded with In_2S_3 microflower surfaces in TEM. The crystal structure of In_2S_3/CdS and elemental composition (S, Cd and In) were shown by high-resolution transmission electron microscopy (HRTEM) (Fig. 1F) and element mapping (Fig. 1G). The In_2S_3 and CdS lattice spacing distances were 0.62 and 0.362 nm, corresponding to the (103) and (100) crystal planes, respectively. As shown in Fig. 1H, with the introduction of CdS, the absorption intensity of In_2S_3/CdS in the visible region was significantly increased. Photoluminescence (PL) was another index of the recombination of photo-generated electrons and holes, where a low PL intensity indicated a low rate of electron-hole recombination [23]. The PL spectra showed a distinct emission peak at 610 nm for both original In_2S_3 and In_2S_3/CdS composites, and the intensity of the composites was much lower, illustrating that the formation of heterojunction suppressed the recombination of photo-generated carriers, which was conducive to the enhancement of photocatalytic activity (Fig. 1I).In Fig. S1, the interaction force between particles was measured by Zeta potential to determine the bonding force of the heterojunction interface [24]. The CdS surface was positively charged, while In_2S_3 had the opposite charge, suggesting that the heterojunction interface achieved stable composite bonding through electrostatic interactions.

The chemical composition and valence state of the surface elements of pure In_2S_3, CdS and In_2S_3/CdS composite were determined by X-ray photoelectron spectroscopy (XPS) [25]. As shown in Fig. S2, Cd, In and S elements have been observed in the full spectrum of the In_2S_3/CdS composite, indicating that the composite was successfully prepared. As observed from the high-resolution spectra of Cd 3d and In 3d (Fig. 2A-B), when In_2S_3 nanoflower was composited with CdS hollow spheres, the characteristic peaks of Cd 3d in the In_2S_3/CdS composite shifted towards higher electron binding energy. Conversely, the peaks of In 3d moved in the opposite direction, suggesting the presence of significant electronic interactions between them. The change of SVs on the surface of the original sample In_2S_3 and In_2S_3/CdS heterojunction was analyzed by

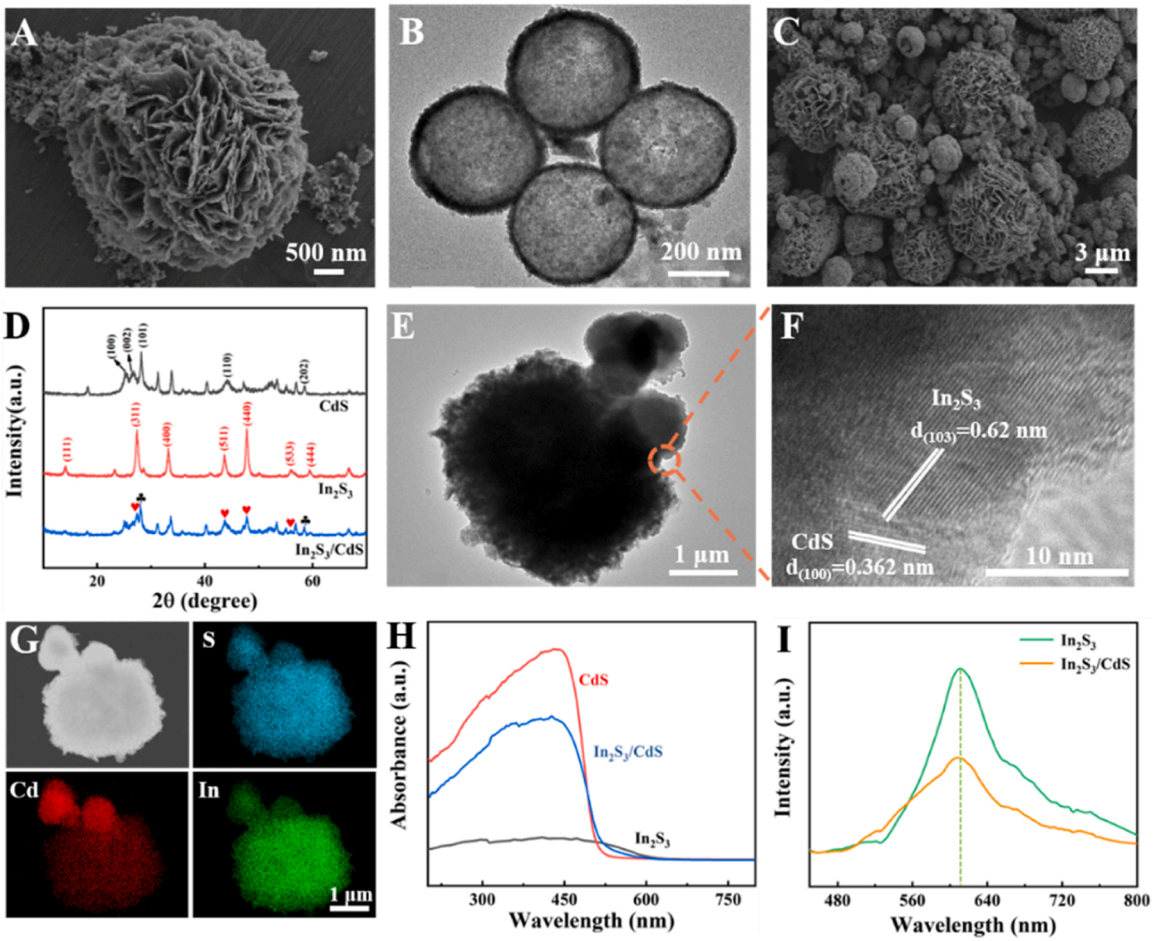

Fig. 1. (A) SEM images of the In_2S_3. (B) TEM images of the CdS. (C) SEM images of the In_2S_3/CdS. (D) XRD patterns of In_2S_3, CdS and In_2S_3/CdS. (E) TEM images of In_2S_3/CdS. (F) HRTEM image of In_2S_3/CdS. (G) Element mapping corresponding to S, Cd and In in the composite material. (H) UV-Vis diffuse reflectance spectroscopy of In_2S_3, CdS and In_2S_3/CdS. (I) PL spectra of the prepared samples.

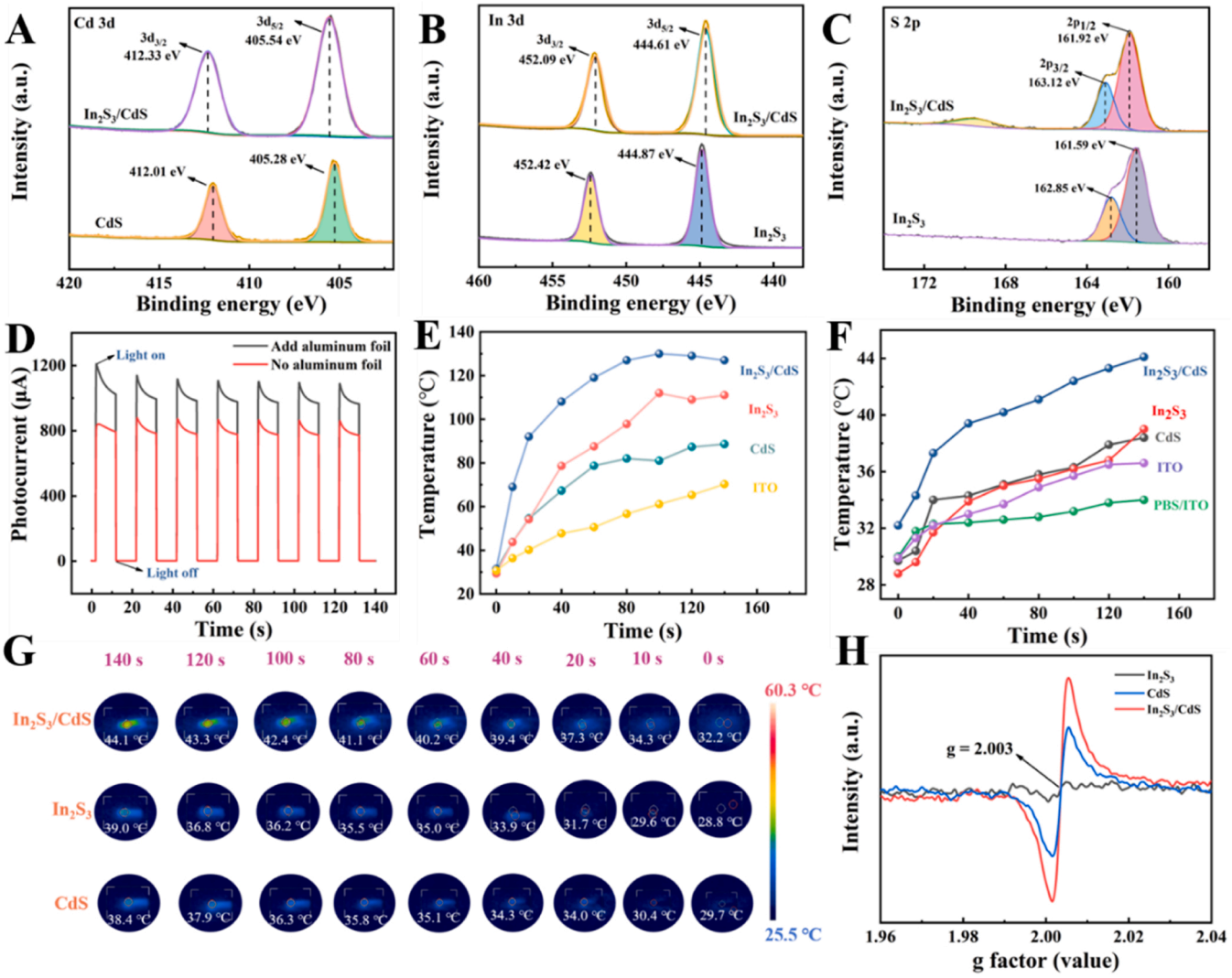

Fig. 2. The high-resolution XPS spectra of (A) Cd 3d, (B) In 3d and (C) S 2p. (D) Photocurrent response of In_2S_3/CdS under Xe lamp illumination. (E) Temperature increment curves under 808 nm laser irradiation (P = 1.5 W). (F) Temperature increment curves of ITO/In_2S_3, ITO/CdS and ITO/In_2S_3/CdS in PBS containing AA. (G) Heating images of ITO/In_2S_3, ITO/CdS and ITO/In_2S_3/CdS under Xe lamp illumination (PBS containing AA). (H) EPR spectra of In_2S_3, CdS and In_2S_3/CdS.

XPS. In Fig. 2C, the S 2p electron binding energy of S $2p_{3/2}$ and S $2p_{1/2}$ were 161.92 eV and 163.12 eV, respectively, while the electron binding energy of In $3d_{5/2}$ and In $3d_{3/2}$ were 444.87 eV and 452.42 eV, respectively. However, on the In_2S_3/CdS heterojunction, the electron binding energy of S 2p shifted to a higher direction, while the signal of In 3d shifted slightly to a lower direction. The peak shift in the opposite direction corresponded to the oxidation of S centers and the reduction of In centers, which strongly confirmed the existence of SVs at the In_2S_3/CdS heterojunction interface [26].

3.2. PEC and photothermal tests of In_2S_3 and In_2S_3/CdS

The transformation of external light energy into thermal energy further influenced the migration of photo-generated carriers. Fig. 2D showed the increase of the photocurrent value to 1.5 times of the original one while using an electrolyzer wrapped with aluminum foil and the standard test. With the continuous irradiation of the light source, the temperature of the buffer solution fluctuates from the initial 32.0 °C to the final 34.1 °C, as shown in Fig. S3. To further investigated the influence of photothermal conversion on the direction of electron flow at the heterojunction interface, measurements were carried out using an 808 nm near-infrared laser, and the change of surface temperature was observed. As shown in Fig. 2E, the photothermal test illumination under 808 nm near-infrared laser irradiation for 140 s revealed that the temperatures of In_2S_3, CdS and In_2S_3/CdS were gradually increased and stabilized. Among them, In_2S_3/CdS has strong absorbance in the near-infrared (NIR) spectrum, showing excellent photothermal performance. Photothermal tests were performed in the phosphate buffer solution under the same conditions, and a thermal imager was used to visualize the temperature changes on the surface of material further (Fig. 2F-G). The above test results indicated that the n-type semiconductor photothermal agent In_2S_3 tended to provide electrons to the ITO electrode and the unique nanoflower structure could expose more active sites, exhibiting efficient anodic photocurrent [27]. Based on this, In_2S_3 transfers excess thermal energy from the environment to the pyroelectric material CdS [18], which accelerates charge transfer and enhances the PEC process [28].

During the illumination process, the changing temperature of the pyroelectric material CdS produced spontaneous polarization, which provided a favorable driving force for carrier separation [29]. Besides that, the SVs in In_2S_3/CdS heterojunction were characterized by an electron paramagnetic resonance spectrometer (EPR). As shown in Fig. 2H, the EPR response of In_2S_3 was almost negligible, indicating the absence of localized unpaired electrons in In_2S_3. In contrast, CdS

samples showed a sharp increase in EPR signal at g = 2.003, confirming abundant SVs in CdS [30]. With the introduction of CdS to construct heterojunction, the EPR signal became increasingly apparent, indicating the formation of more SVs on In_2S_3/CdS. New defect levels of SVs were introduced into the energy band structure of the heterojunction to drive the organized charge migration, consequently enhancing photoelectric conversion efficiency [26].

3.3. Mechanism analysis

Density functional theory (DFT) calculation is an effective method to study the migration of photo-generated carriers in S-scheme heterojunctions. According to the band theory, the work function (Φ) represents the energy difference between the vacuum and the Fermi energy level, which guides the direction of charge transfer in the heterojunction [31]. Based on the calculation of DFT (Fig. 3A-B), the work functions of In_2S_3 (200 crystal plane) and CdS (200 crystal plane) were 5.427 eV and 5.228 eV, respectively. Electrons can flow from the semiconductor with a low work function to the semiconductor with a high work function at the contact surface [32]. In Fig. 3C, when the two semiconductors were in close contact, the Fermi energy level difference drove the transfer of electrons from CdS to In_2S_3 until the Fermi energy levels reached equilibrium [33]. The migration of electron resulted in the formation of the Helmholtz electric double layer structure at the interface of heterojunction. The band edge of In_2S_3 was bent downward due to the electrical gain, while CdS's band edge was bent upwards because of the electron loss. Eventually, the migration of electron at the interfaces of In_2S_3 and CdS led to the formation of an electron accumulation layer and an electron depletion layer, respectively, which is responsible for the establishment of the internal electric field (IEF) [34]. Combining the band gap and conduction band values of In_2S_3 and CdS obtained from the Tauc equation and Mott-Schottky curves (Fig. S4), the above results are consistent with typical S-scheme heterojunction charge transfer paths.

Based on the energy band structure, a potential mechanism was proposed to elucidate how dual-drive forces accelerate the transition of photo-generated carriers within the S-scheme heterojunctions (Fig. 3D). The In_2S_3 nanoflowers converted the excess light energy absorption into thermal energy, which made the temperature of the pyroelectric material CdS fluctuate and produced apparent dipole oscillation. Exposing CdS to both external light and thermal energy accelerated the transport rate of photo-generated carriers and significantly improved the photoelectric response [29]. The defect energy levels of SVs induced CdS photo-generated carriers to transfer to VB of In_2S_3 and recombined with holes, promoting the rapid separation of photo-generated carriers on In_2S_3. Briefly, the photo-generated carriers could be separated and

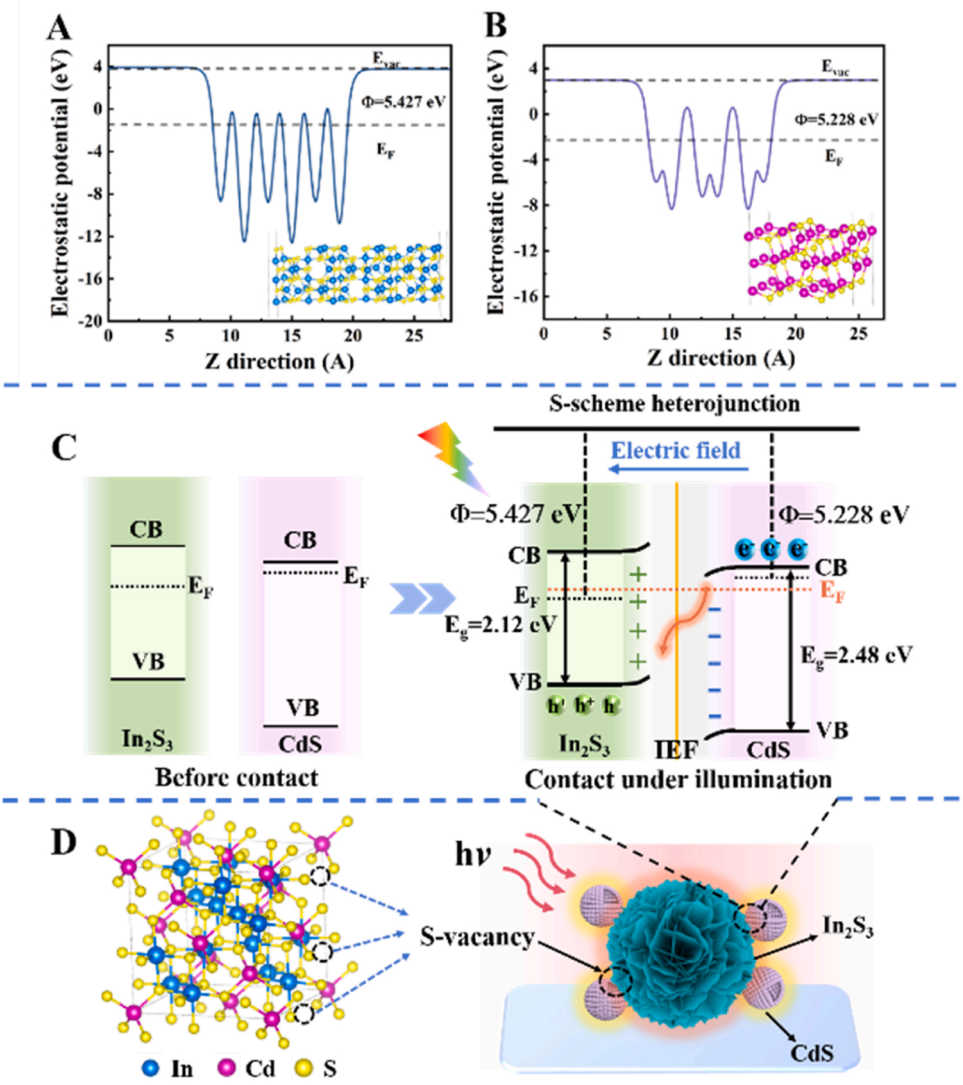

Fig. 3. (A, B) Work functions of In_2S_3 and CdS. (C) Electrons transfer paths of In_2S_3/CdS S-scheme heterojunction. (D) The possible PEC mechanism of In_2S_3/CdS heterojunction.

moved along the S-scheme heterojunction due to the synergistic effect of the photothermoelectric effect and SVs induction at the interface.

3.4. Characterization of PEC sensor construction process

To verify the success of the biosensor preparation, we used the PEC test and electrochemical impedance spectroscopy (EIS) to characterize its construction process [35]. As observed in the Fig. 4A, it showed an excellent anodic photocurrent (curve b) when In_2S_3 was modified on a bare ITO electrode (curve a). The photocurrent of CdS on ITO/In_2S_3 increased significantly (curve c), which could be attributed to the absorption of heat by the photothermal agent In_2S_3 leading to the rapid migration of photo-generated carriers within the pyroelectric semiconductor material (CdS), slowing down the electron-hole recombination rate [36]. In Fig. 4B, due to the increase of protein hindrance, the photocurrent gradually decreased when Ab (curve d), BSA (curve e) and CD44 (curve f) were steadily modified, and the equivalent circuit was fitted to give the corresponding R_{et} value (Table S1). All the above test results demonstrated that the fabricated sensor achieved perfect construction.

3.5. Performance analysis

To evaluate the analytical performance of the biosensor, the PEC response of different concentrations of CD44 to the biosensor was studied under optimal experimental conditions (Fig. S5) [3]. In Fig. 5 A, the anode photocurrent signal decreased as the CD44 antigen concentration increased (from 0.001 ~ 1000 ng mL^{-1}). Besides, we found that the difference between the photocurrent and CD44 concentration logarithm showed a better linear relationship (Fig. 5B) with a linear equation of $I = 386.1 - 74.47 \times \lg c_{CD44}$ ($R^2 = 0.9972$). Compared with other reported methods (Table S2), this PEC sensing platform was preferable for the analytical detection of CD44.

In the practical CD44 detection, stability and selectivity were essential factors in evaluating PEC detection platforms [37]. The photocurrent density and shape barely fluctuated during 21 repetitive switching on/off irradiation cycles, indicating that the PEC platform has good stability (Fig. 5C). Furthermore, selectivity was validated using several potential disruptors (CA72–4, CA125 and HFABP) at 100 ng mL^{-1} concentrations. Satisfactorily, these disturbances all showed a weak effect and only a solution with the target subject could alter the photocurrent signal (Fig. 5D). The results demonstrated that the PEC sensor platform utilizing an internal and external dual-drive strategy exhibited outstanding selectivity towards CD44, thereby ensuring the reliability of detection results in complex samples. The relative standard deviation (RSD) of the sensor reproducibility test in Fig. 5E was 0.48 %, indicating good reproducibility among the sensors. After storing the successfully constructed PEC sensor in a refrigerator at 4 °C for four weeks, the photocurrent remained at 85.2 % of the initial intensity (Fig. 5F), suggesting credible stability.

3.6. Analysis of real samples

To evaluate the performance of the PEC biosensor in actual detection, we tested the recovery of CD44 in serum samples at different concentrations by the spike recovery test. In Table S3, the acceptable recovery rate of CD44 ranged from 99.44 ~ 100.1 % and the RSD was 0.19 ~ 1.8 %. The above results demonstrated that this sensing strategy possessed great potential for the application of CD44 in clinical detection.

4. Conclusions

In summary, a PEC biosensing platform was developed based on the dual-drive strategy to achieve ultrasensitive detection of CD44. The advantages of the designed innovative platform are as follows: (1) The innovative introduction of photothermal materials fully utilized the excess energy in the environment as an external driving force, successfully increasing the photocurrent response of the sensing platform to 1.5 times that of the original. (2) Sulfur vacancies (SVs) functioned as an internal driving force that altered the initial atomic arrangement within the heterojunction, thereby diminishing the impediment to charge transfer and facilitating the induced separation of interfacial charges. (3) In contrast to the conventional heterojunction sensing interface, the developed S-scheme heterojunction established an ordered separation pathway conducive to directed charge transport. In consequence, the well-designed dual-drive strategy offers a novel approach to achieving ultrasensitive detection, which is conducive to facilitating the extensive research of photothermal materials in immunoassays.

Associated content

None.

Supporting information

Materials and instruments; apparatus, Zeta potential of In_2S_3, CdS and In_2S_3/CdS, the band gap values, Mott-Schottky plots, temperature rise curve of buffer solution under xenon lamp irradiation, optimization of experimental conditions for PEC sensor, the R_{et} of EIS in Fig. 2B, comparison of proposed methods for the detection of PD-L1, detection of the PD-L1 in human serum samples and the calculation of LOD.

CRediT authorship contribution statement

Hongmin Ma: Methodology. **Dan Wu:** Supervision. **Hongying Jia:** Writing – review & editing. **Tingting Wu:** Writing – review & editing. **Huangxian Ju:** Supervision, Resources. **Qin Wei:** Writing – review &

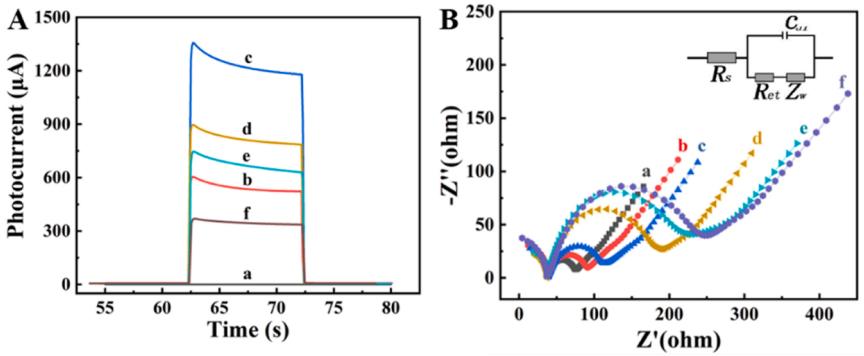

Fig. 4. (A) Photocurrent response and (B) EIS results with (a) ITO, (b) ITO/In_2S_3, (c) ITO/In_2S_3/CdS, (d) ITO/In_2S_3/CdS/Ab, (e) ITO/In_2S_3/CdS/Ab/BSA, (f) ITO/In_2S_3/CdS/Ab/BSA/CD44.

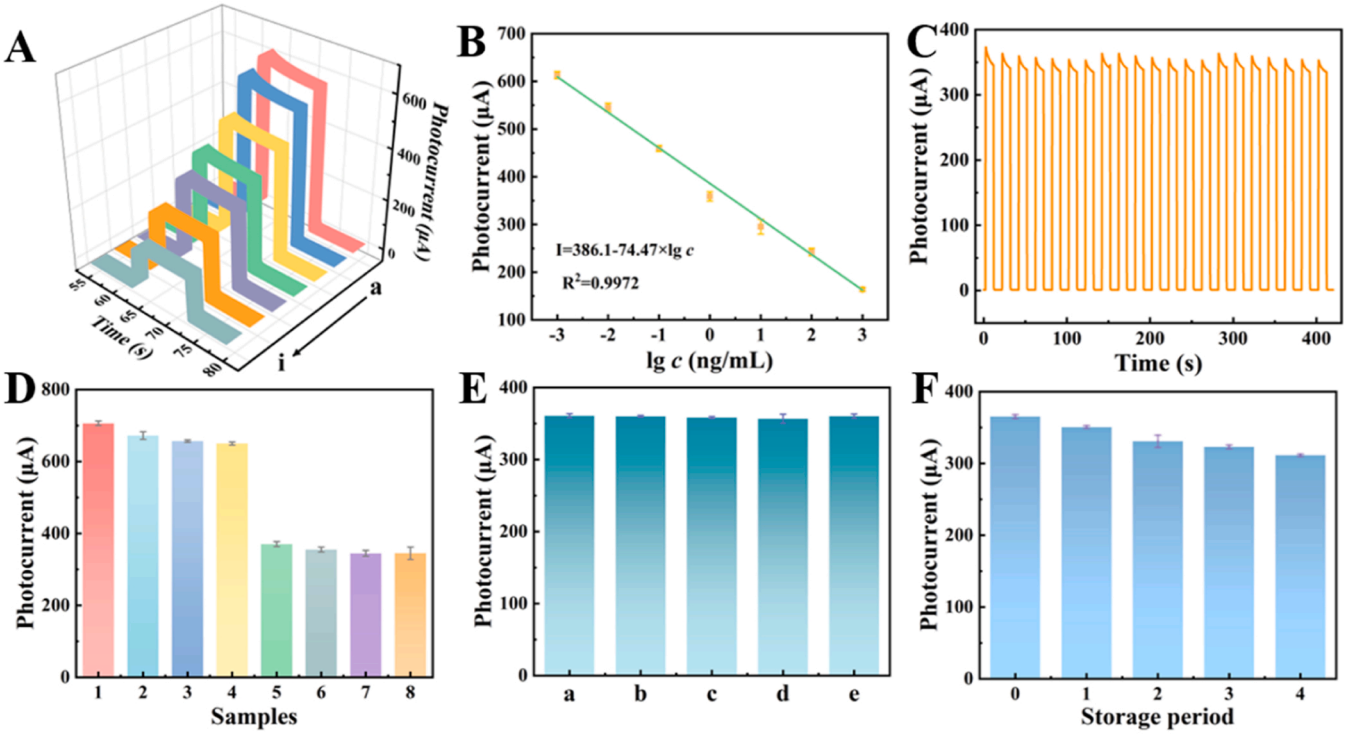

Fig. 5. (A) Photocurrent response of PEC immunosensors with different concentrations of CD44 (0.001 ~ 1000 ng mL^{-1}). (B) Calibration curve. (C) Stability of the PEC sensor in response to CD44 (1 ng mL^{-1}). (D) Selective testing: (1) the blank samples, 100 ng mL^{-1} of (2) CA72–4, (3) CA153 and (4) HFABP were added to the blank samples, and 100 ng mL^{-1} (6) CA72–4, (7) CA153 and (8) HFABP were added to 1 ng mL^{-1} CD44. (E) Reproducibility test. (F) Storage stability. (Error bar, n = 3).

editing, Supervision. **Yamei Li:** Writing – original draft. **Xuan Kuang:** Investigation. **Faying Li:** Data curation.

Declaration of Competing Interest

The authors declare that they have no known competing financial interests or personal relationships that could have appeared to influence the work reported in this paper.

Data Availability

The authors do not have permission to share data.

Acknowledgements

This work was supported by the National Natural Science Foundation of China (22304060, 22274062), the Natural Science Foundation of Shandong Province (ZR2023QB019), the China Postdoctoral Science Foundation (2023M741359, 2023M741360) and the Postdoctoral Fellowship Program of CPSF (GZC20230957).

Appendix A. Supporting information

Supplementary data associated with this article can be found in the online version at doi:10.1016/j.snb.2024.136056.

References

[1] R. Zhang, C. Rejeeth, W. Xu, C. Zhu, X. Liu, J. Wan, et al., Label-free electrochemical sensor for CD44 by ligand-protein interaction, Anal. Chem. 91 (2019) 7078–7085.
[2] P. Ranjan, M. Abubakar Sadique, S. Yadav, R. Khan, An electrochemical immunosensor based on gold-graphene oxide nanocomposites with ionic liquid for detecting the breast cancer CD44 biomarker, ACS Appl. Mater. Interfaces 14 (2022) 20802–20812.
[3] L. Lu, R. Zeng, Q. Lin, X. Huang, D. Tang, Cation exchange reaction-mediated photothermal and polarity-switchable photoelectrochemical dual-readout biosensor, Anal. Chem. 95 (2023) 16335–16342.
[4] L. Zhao, J. Zhou, P. Li, S. Huang, X. Zhu, Y. Zhang, et al., Target-induced photoelectrochemistry and colorimetric dual-mode platform for HIgG based on Ag_2S/SnO_2 composites and CoOOH nanoflakes, Sens. Actuators B Chem. 409 (2024).
[5] J.-H. Zhu, Y.-G. Feng, A.-J. Wang, L.-P. Mei, X. Luo, J.-J. Feng, A signal-on photoelectrochemical aptasensor for chloramphenicol assay based on 3D self-supporting AgI/Ag/BiOI Z-scheme heterojunction arrays, Biosens. Bioelectron. 181 (2021).
[6] Y. Liu, S. Ai, R. Yuan, H. Liu, Defective Se-doped In_2S_3 nanomaterial-based photoelectrochemical biosensor for the ultrasensitive detection of chloramphenicol, Sens. Actuators B Chem. 373 (2022).
[7] B. Zhang, H. Meng, X. Wang, J. Li, H. Chang, W. Wei, Fe^{3+} doped ZnO-Ag photocatalyst for photoelectrochemical sensing platform of ultrasensitive Hg^{2+} detection using exonuclease III-assisted target recycling and DNAzyme-catalyzed amplification, Sens. Actuators B Chem. 255 (2018) 2531–2537.
[8] Y. Cao, K. Lu, Y. Chen, Q. Zheng, C. Huang, N. Jia, In_2O_3/Bi_2S_3 S-scheme heterojunction-driven molecularly imprinted photoelectrochemical sensor for ultrasensitive detection of florfenicol, ACS Appl. Mater. Interfaces 15 (2023) 58397–58405.
[9] Y.-X. Tan, Z.-M. Chai, B.-H. Wang, S. Tian, X.-X. Deng, Z.-J. Bai, et al., Boosted photocatalytic oxidation of toluene into benzaldehyde on $CdIn_2S_4$-CdS: synergetic effect of compact heterojunction and S-vacancy, ACS Catal. 11 (2021) 2492–2503.
[10] Y. Liu, X. Lan, J. Xu, W. Zhou, C. Liu, C. Liu, et al., Organic/inorganic hybrid boosting energy harvesting based on the photothermoelectric effect, ACS Appl. Mater. Interfaces 13 (2021) 43155–43162.
[11] X. Qi, Y. Xiang, E. Cai, X. Ge, X. Chen, W. Zhang, et al., Inorganic–organic hybrid nanomaterials for photothermal antibacterial therapy, Coord. Chem. Rev. 496 (2023).
[12] D. Wang, Y. Zheng, H. Zhao, X. Zhu, D. Ye, Y. Yang, et al., Core–shell β-SiC@PPCN heterojunction for promoting photo-thermo catalytic hydrogen production, ACS Catal. 13 (2023) 10104–10114.
[13] S. Zhang, D. Chen, Z. Liu, M. Ruan, Z. Guo, Novel strategy for efficient water splitting through pyro-electric and pyro-photo-electric catalysis of $BaTiO_3$ by using thermal resource and solar energy, Appl. Catal. B Environ. Energy 284 (2021).
[14] Z. Yu, W.K. Chan, Y. Zhang, T.T.Y. Tan, Near-infrared-II activated inorganic photothermal nanomedicines, Biomaterials 269 (2021).
[15] Y. Liu, J. Shang, T. Zhu, Enhanced thermal-assisted photocatalytic CO_2 reduction by RGO/H-CN two-dimensional heterojunction, J. Mater. Sci. Technol. 176 (2024) 36–47.

[16] C. Wang, H. Ma, Y. Tian, A. Jiao, M. Zhang, L. Zheng, et al., Polymeric layered semiconductor-supported black nano-sandwiches with synergistic photo-thermal catalysis for efficient wastewater decontamination, Chem. Eng. J. 446 (2022).
[17] F.L. Meng, G. Yilmaz, T.P. Ding, M. Gao, G.W. Ho, A hybrid solar absorber–electrocatalytic N-doped carbon/alloy/semiconductor electrode for localized photothermic electrocatalysis, Adv. Mater. 31 (2019).
[18] M. Zhang, Q. Hu, K. Ma, Y. Ding, C. Li, Pyroelectric effect in CdS nanorods decorated with a molecular Co-catalyst for hydrogen evolution, Nano Energy 73 (2020).
[19] J. Bai, W. Chen, L. Hao, R. Shen, P. Zhang, N. Li, et al., Assembling Ti_3C_2 MXene into $ZnIn_2S_4$-$NiSe_2$ S-scheme heterojunction with multiple charge transfer channels for accelerated photocatalytic H_2 generation, Chem. Eng. J. 447 (2022).
[20] Y. Liu, C. Chen, Y. He, Z. Zhang, M. Li, C. Li, et al., Rich Indium-vacancies In_2S_3 with atomic p–n homojunction for boosting photocatalytic multifunctional properties, Small 18 (2022).
[21] X. Chen, Z. Liu, M. Ruan, C. Wang, Z. Guo, Synergistic mechanism of 0D internal and surface defects regulation coupled with pyroelectric effects for optimizing the photoelectrocatalytic properties of CdS, ChemCatChem (2023).
[22] X. Wang, X. Wang, J. Huang, S. Li, A. Meng, Z. Li, Interfacial chemical bond and internal electric field modulated Z-scheme Sv-$ZnIn_2S_4$/$MoSe_2$ photocatalyst for efficient hydrogen evolution, Nat. Commun. 12 (2021).
[23] Y. Qin, J. Zhang, R. Tan, Z. Wu, M. Liu, J. Li, et al., Small-molecule probe-induced In situ-sensitized photoelectrochemical biosensor for monitoring α-glucosidase activity, ACS Sens. 8 (2023) 3257–3263.
[24] X. Liu, J. Xu, F. Li, Z. Liu, S. Xu, Construction S-scheme of 2D nanosheets /1D nanorod heterojunction with compact interface contact by electrostatic self-assembly for efficient photocatalytic hydrogen evolution, Catal. Lett. (2023).
[25] M. Zhang, H. Xue, X. Han, Z. Zhang, Y. Jiang, Y. Deng, et al., Accelerate charge separation in Cu_2O/MoO_2 photocathode for photoelectrocatalytic hydrogen evolution, J. Colloid Interface Sci. 650 (2023) 284–293.
[26] S. Zhang, X. Liu, C. Liu, S. Luo, L. Wang, T. Cai, et al., MoS_2 quantum dot growth induced by S vacancies in a $ZnIn_2S_4$ monolayer: atomic-level heterostructure for photocatalytic hydrogen production, ACS Nano 12 (2017) 751–758.
[27] C.-H. Ho, Y.-P. Wang, NIR and UV enhanced photon detector made by diindium trichalcogenides, Opt. Mater. Expres 3 (2013).
[28] K. Wang, Z. Xing, D. Meng, S. Zhang, Z. Li, K. Pan, et al., Hollow $MoSe_2$@Bi_2S_3/CdS core-shell nanostructure as dual Z-Scheme heterojunctions with enhanced full spectrum photocatalytic-photothermal performance, Appl. Catal. B Environ. Energy 281 (2021).
[29] M. Li, J. Sun, G. Chen, S. Yao, B. Cong, P. Liu, Construction photothermal/pyroelectric property of hollow FeS_2/Bi_2S_3 nanostructure with enhanced full spectrum photocatalytic activity, Appl. Catal. B Environ. Energy 298 (2021).
[30] C. Du, Q. Zhang, Z. Lin, B. Yan, C. Xia, G. Yang, Half-unit-cell $ZnIn_2S_4$ monolayer with sulfur vacancies for photocatalytic hydrogen evolution, Appl. Catal. B Environ. Energy 248 (2019) 193–201.
[31] J. Xi, X. Liu, L. Zhang, Z. Zhang, J. Zhuo, T. Du, et al., Engineering of Schottky heterojunction in Ru@Bi_2S_3/Nb_2C MXene based on work function with enhanced carrier separation for promoted sterilization, Chem. Eng. J. 473 (2023).
[32] Z. Jin, T. Wang, E. Cui, X. Yang, Constructing a tandem heterojunction: S-scheme heterojunction and Ohmic junction based on graphdiyne, synergistically optimizing photocatalytic hydrogen evolution, Chem. Eng. J. 477 (2023).
[33] S. Zhao, J. Jiang, C. Zhang, F. Chen, Y. Song, Y. Tang, Construction of a novel double S-scheme heterojunction CeO_2/g-C_3N_4/Bi_2O_4 for significantly boosted degradation of tetracycline: Insight into the dual charge transfer mode, Chem. Eng. J. 479 (2024).
[34] B. Zhu, J. Sun, Y. Zhao, L. Zhang, J. Yu, Construction of 2D S-Scheme heterojunction photocatalyst, Adv. Mater. (2023).
[35] B. Fan, Q. Fan, M. Cui, T. Wu, J. Wang, H. Ma, et al., Photoelectrochemical biosensor for sensitive detection of soluble CD44 based on the facile construction of a poly(ethylene glycol)/hyaluronic acid hybrid antifouling interface, ACS Appl. Mater. Interfaces 11 (2019) 24764–24770.
[36] L. Huang, J. Chen, Z. Yu, D. Tang, Self-powered temperature sensor with seebeck effect transduction for photothermal–thermoelectric coupled immunoassay, Anal. Chem. 92 (2020) 2809–2814.
[37] X. Chen, M. Yin, R. Ge, J. Wei, T. Jiao, Q. Chen, et al., Insight into a target-induced photocurrent-polarity-switching photoelectrochemical immunoassay for ultrasensitive detection of Escherichia coli O157:H7, Anal. Chem. 95 (2023) 2698–2705.

Yamei Li is a PhD candidate at the School of Chemistry and Chemical Engineering, University of Jinan. Her current researches are photoelectrochemical sensor and nanomaterials.

Xuan Kuang is a lecturer at the School of Chemistry and Chemical Engineering, University of Jinan. Her main research interest is the construction and properties of chiral metal-organic frame materials and their derivatives.

Faying Li is a lecturer at Shandong First Medical University. His main research interest is the research and design of photoelectric sensing interfaces.

Hongmin Ma received both his B.S. and M.S. degree in Applied Chemistry from University of Jinan in 2005 and 2008 respectively. And he has received his Ph.D. degree in Colloid and Interface Chemistry at Shandong University, investigating self-assembly at all scales at surfaces in 2011. Now, he is a professor at University of Jinan, interested in the assembly of nano-composites and the construction of ordered porous films as well as their analytical applications.

Dan Wu a professor and received the Ph.D. degree from Shandong University in 2005. She dedicates to the surfactant and biological macromolecules interaction. And now she also studies the role of surfactant in electrochemical immunosensor.

Hongying Jia is currently a PhD candidate in the School of Chemistry and Chemical Engineering, University of Jinan. Her current research interests are the application of electroluminescent sensors and nanomaterials.

Tingting Wu received her B.S. and M.S. degrees in University of Jinan in 2016 and 2019 respectively. She is currently a Ph.D.student in School of Chemistry and Chemical Engineering, University of Jinan. Her current researches are photoelectrochemical sensor and nanomaterials.

Huangxian Ju is a Changjiang Professor and the director of State Key Laboratory of Analytical Chemistry for Life Science in Nanjing University. His research interests focus on bioanalytical chemistry, nanobiosensing and molecular diagnostics. He has published 13 books and 918 papers in different journals with SCIE h-index of 106 (>44,300 citations) and Google Scholar h-index of 117 (> 53000 citations).

Qin Wei, a professor and DSc, has devoted herself to analytical teaching and scientific research. Her main research interests are the determination of protein and nucleic acid by photometry and the electrochemical immunosensor preparation. She has published over 200 articles on analysis, immunosensor and applied successfully for many research projects, such as Analytical Chemistry, Advanced Functional Materials, Chemical Communication, Biosensors & Bioelectronics, Journal of Materials Chemistry A, and ACS Applied Materials & Interfaces.